Self-Assembling Block Copolymer Systems Involving Competing Length Scales: A Route toward Responsive Materials

Rikkert Nap,[†] Igor Erukhimovich,[‡] and Gerrit ten Brinke*,[†]

Department of Polymer Chemistry and Materials Science Centre, University of Groningen, Nijenborgh 4, 9747 AG Groningen, The Netherlands, and Chair of Physics of Polymers and Crystals, Physics Department, Moscow State University, Leninskie Gory, 119992 Moscow, Russia

Received November 6, 2003; Revised Manuscript Received March 3, 2004

ABSTRACT: The phase behavior of block copolymers melts involving competing length scales, i.e., able to microphase separate on two different length scales, is theoretically investigated using a self-consistent field approach. The specific block copolymers studied consist of a linear A-block linked to an alternating (A-*alt*-B)-block. The large length scale microphase separation is closely related to the overall length scale of the block copolymer, whereas the short length scale microphase separation is associated with the length scale of the repeat unit of the alternating block. Because of the presence of competing intrinsic length scales, the periodicity of the lamellar structure is extremely temperature sensitive. For a range of polymer compositions a first-order phase transition occurs from a lamellar morphology with a large periodicity to a lamellar or hexagonal morphology with a much smaller periodicity. Such phase transitions could potentially form the basis for responsive materials.

1. Introduction

Simple AB-block copolymer melts microphase separate with *one* characteristic length scale. However, if more than two monomer types are involved, microphase separation frequently occurs at different length scales.[1−7] Several examples can be found in the experimental work of Ikkala and ten Brinke and co-workers. There,[4−6] linear−comb diblock copolymers are investigated consisting of a polystyrene-*block*-poly(4-vinylpyridine) (PS-*b*-P4VP) diblock copolymer with side chains (e.g., pentadecylphenol, PDP) attached by hydrogen bonds to the P4VP-block. The resulting linear−comb diblock copolymers show typical two length scale hierarchical structure-*within*-structure morphologies. The PS-blocks microphase separate from the P4VP(PDP)-blocks, giving rise to the well-known classical morphologies depending on the volume fraction of either block. This structure corresponds to the large length scale ordering, and the order−disorder transition temperature is, if present at all, very high. Inside the P4VP(PDP) domains an additional short length scale lamellar ordering takes place below the order−disorder transition at ca. 60 °C. The structure-*within*-structure formation of these comb-shaped supramolecules can be used to prepare materials with interesting electronic and photonic properties. For example, upon selective "doping" of one block, temperature-dependent proton conductivity can be suitably based on a sequence of phase transitions.[8,9] The self-organization of similar linear−comb diblock supramolecules using dodecylbenzenesulfonic acid (DBSA) and high molar mass diblock copolymers, PS-*block*-P4VP-(DBSA), leads to a particularly large lamellar periodicity in excess of 100 nm with a strong reflectivity around 460 nm; i.e., an incomplete photonic band-gap opens.[10,11]

Structure formation involving competing length scales is only possible for systems that can phase separate in more than one way. An interesting example, very recently discussed by Erukhimovich et al.,[12] concerned a mixture of AC-diblock and ABC-triblock copolymers. Other possibilities, which will form the main subject of this paper, are based on pure copolymer melts (not mixtures) of copolymer molecules with an architecture that involves more than one intrinsic length scale. The most simple example consists of ABC-triblock copolymers, which indeed formed the subject of many experimental and theoretical investigations during recent years.[1,3,7,13−16] By selecting appropriate block lengths, a variety of structures have been produced. Such systems are hard to analyze systematically because three different Flory−Huggins interaction parameters (χ_{AB}, χ_{AC}, χ_{BC}) and two different composition variables (f_A, f_B) are involved.

Interestingly enough, when competing length scales is the topic of real interest, the use of two chemically different monomers only turns out to be a more natural choice. In the case of the aforementioned linear−comb PS-*block*-P4VP(PDP) supramolecules self-organization leads to hierarchical structures characterized by two length scales; however, the self-assembly does not involve a real competition between the two length scales. The large length scale is formed at high temperatures where upon cooling the short length scale structure is formed inside the domains that contain the comb-shaped blocks. Genuine competing length scales require only two chemically different monomers. By selecting diblock copolymer-like architectures with one block being a homopolymer and the other block being essentially a multiblock, two intrinsic length scales are introduced in a most natural way. In particular, the use of a multiblock as one of the two blocks almost automatically introduces a length scale that is an order of magnitude smaller than the length scale corresponding to the diblock structure. Typical examples are diblock copolymers consisting of an A-homopolymer block and either an A-*graft*-B block or an A-*alt*-B block denoted as A_m-*b*-(A-*g*-B)$_n$ or A_m-*b*-(B-*b*-A)$_n$. These copolymers will be referred to as linear−comb block copolymers and linear−alternating block copolymers, respectively. A schematic picture of the linear−alternating block copolymer architecture, which forms the subject of the present paper, is shown in Figure 1.

Because of the architecture of the molecule, microphase separation is feasible at two different length

[†] University of Groningen.
[‡] Moscow State University.

10.1021/ma0356663 CCC: $27.50
Published on Web 04/29/2004

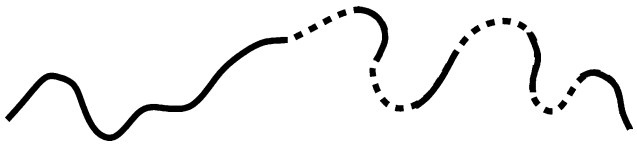

Figure 1. Linear−alternating block copolymer architectures considered.

scales, which loosely speaking correspond to microphase separation "between" the linear A-block and the AB-block and "inside" the AB-multiblock. The first possibility resembles that of a diblock copolymer melt, and the characteristic length scale corresponds to the length scale of the whole molecule. The second possibility involves microphase separation on the level of the alternating block. The A- and B-blocks of the alternating block phase separate from each other, and the linear A-block resides inside the A-phase formed by the alternating A-blocks. In the situation analyzed further on in detail, the alternating block itself is taken to have a symmetric composition. However, the presence of the extra A-monomers of the linear block, over that of the alternating block, in the A-phase introduces an asymmetry, implying that in this case the A- and B-domains will not be of equal size. Still, the characteristic length scale of the self-organized structure will be dominated by the length scale of *one* repeat unit of the alternating block.

Depending on the number of repeat units (n) of the alternating block and the length of the linear A-block (m), the phase behavior is dominated by either of the two length scales, or these length scales are competing for dominance. A stability analysis of the disordered melt[17] demonstrated that the $n-m$ parameter space displays a bifurcation point. Above the bifurcation point a region exists where both length scales are dominately present: the structure factor exhibits two correlation hole peaks. Note that the "spinodal" behavior of the linear−alternating and the linear−comb block copolymers is completely analogous. In an ensuing article,[18] we examined the stability of the ordered phases of linear−comb (rather than the linear−alternating considered here) block copolymer melts within the framework of the weak segregation theory. Such an analysis is only valid near the order−disorder transition temperature (ODT) because the weak segregation theory involves a Landau expansion of the free energy up to fourth order in the concentration profile together with the representation of the concentration profile with only *one* dominant wave vector. In particular, the second approximation proved to be very restrictive for the systems under consideration. Consequently, we were only able to calculate the free energy in the weak segregation theory for those values of n and m where the phase behavior is dominated by one length scale, which moreover is *not* influenced by the second one. To extend the analysis beyond the ODT and to investigate the effect of competition between both length scales, we decided to apply the self-consistent field approach. The paper is organized as follows. In section 2, the theory is outlined and the pertinent system parameters are defined, and in section 3 the results are presented and discussed.

2. Theory

Here we briefly review the self-consistent field theory[19−22] for linear block copolymer melts. For more detailed information see e.g. refs 22−24.

We consider an incompressible polymer melt consisting of n_p AB linear block copolymers of degree of polymerization N. The volume of an A-monomer as well as a B-monomer is $1/\rho_0$. Thus, the total volume of the system equals $V = n_p N/\rho_0$. The configuration of the ith polymer is represented by a contour curve $\mathbf{r}_i(s)$. The variable s is proportional to the arc length along the contour of the polymer, where s is scaled such that $s \in [0, 1]$. The architecture or composition of the block copolymer is defined by the function $\sigma_\alpha(s)$, which equals one if monomer s is of type α and is zero otherwise.

We suppose that the linear−alternating block copolymer A_m-*b*-(B-*b*-A)$_n$ consists of a linear A-block and an AB-alternating block.[17] The alternating block consists of n identical AB-blocks of symmetric composition, i.e., with equal number of A- and B-monomers. Hence, the A- and B-blocks of one repeat unit of the alternating block have equal degrees of polymerization, denoted as d. The length of the linear block, expressed in units of d, is m. Therefore, the total length of the polymer is $N = (2n + m)d$. The $\sigma_A(s)$ for the linear−alternating block copolymer is given by

$$\sigma_A(s) = \begin{cases} 1 & 0 \le t \le m \quad \text{linear block} \\ 0 & m + 2i \le t \le m + 2i + 1 \quad \text{alternating block} \\ 1 & m + 2i + 1 \le t \le m + 2i + 2 \quad \text{alternating block} \end{cases} \tag{1}$$

where $s = t/(2n + m)$ and $i \in 0, 1, ..., n - 1$. Note that $\sigma_B(s) = 1 - \sigma_A(s)$. Assuming the interaction is described by the familiar Flory−Huggins expression, incompressibility, and Gaussian statistics, the following free energy functional F can be derived[22]

$$\frac{F}{n_p kT} = \frac{F}{kT}\frac{N}{V\rho_0} = -\ln Q + \frac{1}{V}\int d\mathbf{r}\, [\chi N \Phi_A \Phi_B - \{W_A \Phi_A + W_B \Phi_B + \Xi(1 - \phi_A - \phi_B)\}] \tag{2}$$

The functional $Q = Q[W_A, W_B]$

$$Q = \int D\mathbf{r}\, P[\mathbf{r}; 0; 1] \exp[-\int_0^1 ds\, \{\sigma_A(s)\, W_A(\mathbf{r}(s)) + \sigma_B(s)\, W_B(\mathbf{r}(s))\}] \tag{3}$$

is the partition function of *one* polymer subject to the external fields W_A and W_B acting on the A and the B monomers, respectively. Here P is the Gaussian weight distribution function. The functions Φ_α correspond to monomer density functions. The function Ξ enforces the incompressibility. The mean-field free energy is given by the extremum of $F[\Phi_A, \Phi_B, W_A, W_B, \Xi]$ and denoted by $F[\phi_A, \phi_B, w_A, w_B, \xi]$. The equations determining this extremum are

$$w_A(\mathbf{r}) = \chi N \phi_B(\mathbf{r}) + \xi(\mathbf{r}) \tag{4}$$

$$w_B(\mathbf{r}) = \chi N \phi_A(\mathbf{r}) + \xi(\mathbf{r}) \tag{5}$$

$$\phi_A(\mathbf{r}) = -\frac{V}{Q}\frac{\delta Q}{\delta w_A(\mathbf{r})} \tag{6}$$

$$\phi_B(\mathbf{r}) = -\frac{V}{Q}\frac{\delta Q}{\delta w_B(\mathbf{r})} \tag{7}$$

$$1 = \phi_A(\mathbf{r}) + \phi_B(\mathbf{r}) \tag{8}$$

The preceding equations show that the densities are related to the functional derivatives of $Q[w_A,w_B]$. Once the partition function Q is known, the set of eqs 4−8 can be solved. To this end, the partition function Q is rewritten as $Q \equiv \int d\mathbf{r}\ q(\mathbf{r},1)$, where $q(\mathbf{r},s)$ is the end-segment distribution function. This end-segment distribution function satisfies the modified diffusion equation

$$\frac{\partial q(\mathbf{r},s)}{\partial s} = \frac{1}{6}Na^2\nabla^2 q(\mathbf{r},s) - w(\mathbf{r},s)\, q(\mathbf{r},s) \qquad (9)$$

where $w(\mathbf{r},s) = w_A(\mathbf{r})\,\sigma_A(s) + w_B(\mathbf{r})\,\sigma_B(s)$ and its boundary condition is $q(\mathbf{r},0) = 1$. There exists a second end-segment distribution function $\bar{q}(\mathbf{r},s)$ also satisfying eq 9 apart from an additional minus on the left-hand side and a different boundary condition: $\bar{q}(\mathbf{r},1) = 1$. With the above definitions the monomer density functions become

$$\phi_\alpha(\mathbf{r}) = \frac{V}{Q}\int_0^1 ds\ \sigma_\alpha(s)\, q(\mathbf{r},s)\, \bar{q}(\mathbf{r},s) \qquad (10)$$

To obtain a solution, eqs 4−10 need to be solved numerically. This is done by reformulating these equations in the reciprocal space of a set of basis functions, i.e., writing every spatial depended function as $f(\mathbf{r}) = \sum_i f_i \varphi_i(\mathbf{r})$. These basis functions $\varphi_i(\mathbf{r})$ satisfy the symmetry properties of a given spatial structure and are eigenfunctions of the Laplace operator: $\nabla^2\varphi_i(\mathbf{r}) = -\lambda_i/D^2\varphi_i(\mathbf{r})$. The variable D is the periodicity of the structure under consideration. Within the reciprocal space of the basis functions the partial differential equation becomes a differential equation of the form

$$\frac{dq_i(s)}{ds} = \sum_\alpha\sum_j A_{\alpha,ij}\sigma_\alpha(s)\, q_j(s) \qquad (11)$$

where

$$A_{\alpha,ij} = -\frac{1}{6}Na^2\lambda_i D^{-2}\delta_{ij} - \sum_k w_{\alpha,k}\Gamma_{ijk},$$
$$\Gamma_{ijk} = \frac{1}{V}\int d\mathbf{r}\ \varphi_i(\mathbf{r})\,\varphi_j(\mathbf{r})\,\varphi_k(\mathbf{r}) \qquad (12)$$

This set of equations can be readily solved through orthogonal transformations that diagonalize A_A and A_B.[25−27] By substituting the expressions for q_i and $\bar{q}_i$ into the density function, the integral over s can be carried out analytically. The density functions, i.e $\phi_\alpha(r) = \sum_i \phi_{\alpha,i}\varphi_i(\mathbf{r})$, are expressed in the eigenvalues and eigenvectors of the matrices A_A and A_B.[26,28] The remaining self-consistent field equations become, in the reciprocal space of the basis functions

$$w_{A,i} = \chi N\phi_{B,i} + \xi_i \qquad (13)$$

$$w_{B,i} = \chi N\phi_{A,i} + \xi_i \qquad (14)$$

$$\delta_{1i} = \phi_{A,i} + \phi_{B,i} \qquad (15)$$

Combining the above equations gives for $i \neq 1$

$$\phi_{A,i} = -\phi_{B,i} = (w_{B,i} - w_{A,i})/2\chi N \qquad (16)$$

$$\xi_i = (w_{A,i} + w_{B,i})/2 \qquad (17)$$

For $i = 1$ we may set $\xi_1 = 0$, which gives $w_{A,1} = \chi N\phi_{B,1}$ and $w_{B,1} = \chi N\phi_{A,1}$ with $\phi_{\alpha,1} = f_\alpha$, where f_α is the volume fraction of monomer type α.

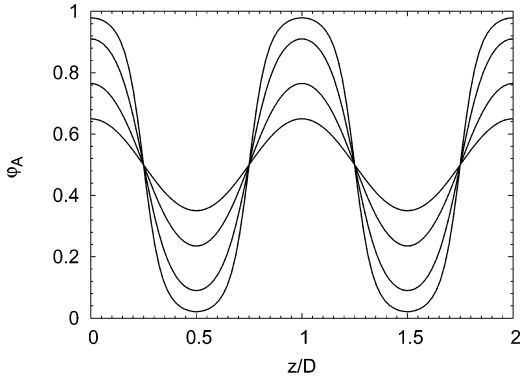

Figure 2. A-density profiles of the lamellar structure of a symmetric alternating block copolymer (A-*b*-B)$_{10}$ with $n = 10$ repeat units. At $z = 0$, the profiles correspond from bottom to top to $\chi(2d) = 15$, 16, 20, and 30.

The self-consistent field equations can now be solved iteratively. We start with an initial guess for $w_{\alpha,i}$, enabling us to compute q_i and $\bar{q}_i$ (the eigenvalues and eigenvectors) from which the densities $\phi_{\alpha,i}$ are calculated. Subsequently, the external fields $w_{\alpha,i}$ are adjusted such that the densities obtained for the external fields satisfy eq 16. Having found a solution for the self-consistent field equations, the free energy is calculated. For an ordered structure the free energy has to be minimized with respect to the periodicity D, and finally a phase diagram is constructed by comparing the free energies of different structures and selecting the structure with minimal free energy as the equilibrium state.

Two numerical iterations schemes have been used to solve the nonlinear self-consistent field equations: a Picard-like algorithm and the Broyden algorithm.[27,29−31] In a Picard iteration new external fields are obtained by a linear combination of the old and new external fields and densities, which are then used in the next iteration step. The Broyden algorithm is essentially a quasi-Newton algorithm.[31] We mostly employed the Picard iteration method to solve the SCF equations.

3. Results and Discussion

Before we present the results of the self-consistent field calculations of the linear−alternating block copolymer melts, we first briefly consider purely alternating block copolymer melts. Their phase behavior is generic for block copolymer systems having only *one* intrinsic length scale. It will be of interest to contrast it with the phase behavior of melts of linear−alternating block copolymers, characterized by *two* intrinsic length scales. Particular attention will be given to the periodicity of the lamellar morphology.

3.1. Phase Behavior of Alternating Block Copolymer Melts. We consider an alternating block copolymer melt (A-*b*-B)$_n$ with A- and B-blocks having the same number of segments d. In Figure 2 A-density profiles for a microphase-separated symmetric alternating block copolymer melt ($n = 10$) obtained by the SCF approach are shown for several degrees of segregation. Symmetry considerations and calculations with the weak-segregation theory[32] as well as the self-consistent field theory[25,33] and experiments[34−38] show that the equilibrium phase morphology for a symmetric alternating block is the lamellar structure. This is also confirmed by our self-consistent field calculations, through

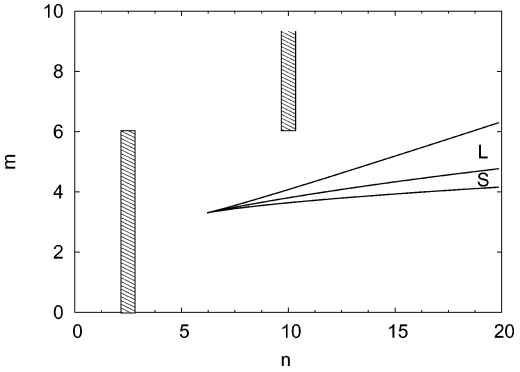

Figure 3. Classification or bifurcation diagram. The dashed areas indicate the systems considered in this paper; *n* refers to the number of repeat units, and *m* indicates the relative length of the linear block.

a comparison of the free energies of the lamellar ($\bar{1}$), cylindrical ($p6\bar{m}m$ and $p4mm$), and cubical structures, ($Im\bar{3}m$ and $Fm\bar{3}m$). The variable $\chi 2d$ controls the degree of segregation between the A- and B-blocks, as is clearly demonstrated in Figure 2. Upon increasing $\chi 2d$, that is decreasing the temperature, the amplitude (maximum) of the density profile becomes larger, and the interfaces between the A- and B-domains become sharper and the periodicity of the lamellar structure increases.[39,40] Thus, upon cooling the melt passes from the weak, via the intermediate, to the strong segregation regime.

Because of the increased complexity of the alternating block copolymers, their conformation behavior is more complicated as compared to diblock copolymers. The molecules are able to form loops and bridges. However, the most important observations is the following: microphase separation of a melt of alternating block copolymers is governed by the degree of polymerization or length of one repeat unit, which only in the case of diblock copolymers coincides with the overall length of the polymer.[33,36,41,42]

Having discussed the phase behavior of alternating block copolymers, we are now in a position to discuss the results obtained for linear−alternating block copolymers using SCFT calculations.

3.2. Phase Behavior of Linear−Alternating Block Copolymers. Figure 3 shows the (n, m) classification or bifurcation diagram for linear−alternating block copolymers of the form A_m-*b*-(B-*b*-A)$_n$ obtained by a stability analysis employing the RPA approximation (see ref 17). Here, the A- and B-blocks are assumed to have equal length d, and the linear A-block has a length md. Inside region S and L the structure factor shows two maxima at wave vectors q_s and q_l ($q_s > q_l$). Inside S the absolute maximum is at q_s, and inside L it is at q_l. Both maxima have the same value on the dividing line. Outside region S and L the structure factor has only one maximum located either at q_s or q_l. (Similiar spinodal behavior is observed in refs 12 and 43; however, all these systems involve mixtures.)

A complete investigation of the parameter space of n and m is clearly impossible since the numerical SCF calculations consume a considerable amount of CPU time. Instead, we focus on a series of systems that already clearly display the influence of two competing length scales but are still relatively easy to analyze. These are indicated in Figure 3 by the dashed areas. Despite the fact that the systems are outside the bifurcation region, they do already show intriguing phase behavior due to a competition between length scales occurring at *intermediate* (rather than weak) segregation conditions.

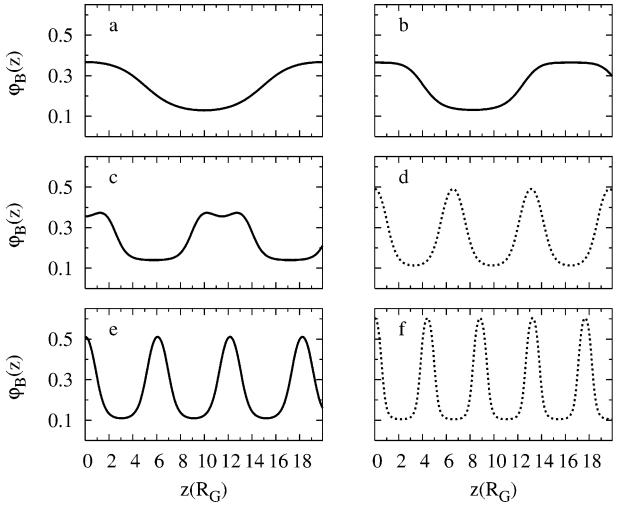

Figure 4. B-density profiles of the lamellar structure of the linear−alternating block copolymer A_{20}-*b*-(B-*b*-A)$_{10}$ for increasing χd. The density profiles (a), (b), (c), (d), (e), and (f) correspond to $\chi d = 2.5$, 5, 11, 11, 11.5, and 22.5, respectively. The solid profiles denote stable lamellar structures, whereas the dotted ones correspond to metastable structures.

First we consider (n, m) = (10, 20). The number of repeat units of the alternating block is chosen such that there is a considerable difference between the two intrinsic length scales. A rough estimate shows that the large length scale is almost an order of magnitude larger than the small length scale:

$$\frac{q_s}{q_l} \simeq \frac{R_G(N)}{R_G(d)} = \sqrt{2n + m} \approx 6 \qquad (18)$$

Here $R_G(M) = \sqrt{1/6a^2M}$ corresponds to the radius of gyration of a chain of length M. The length of the linear block is chosen such that it is equal to the length of the complete alternating block, i.e., $md = 2nd$. The structure factor of the A_{20}-*b*-(B-*b*-A)$_{10}$ shows only one maximum located at q_l. Consequently, for this system a large length scale, diblock-like, phase behavior close to the ODT is expected. By virtue of this stability analysis and the fact that the molecule is symmetric, i.e., $md = 2nd$, the anticipated equilibrium morphology near the ODT is a symmetric lamellar structure, as the calculations confirmed.

To explain and illustrate the structure development of the A_{20}-*b*-(B-*b*-A)$_{10}$ melt, a number of lamellar density profiles are presented in Figure 4. They show the density profiles at different stages of segregation. Figure 4a presents the lamellar density profile at a temperature relatively close to the ODT temperature, which is given by $(\chi d)_{ODT} \simeq 1.095 \pm 0.002$ and $D = (3.174 \pm 0.001)R_G(N)$. This SCFT result is in agreement with the spinodal value of $(\chi d)_s = 1.0934$ with $D^* = 3.17155R_G(N)$. Initially, on cooling the melt still behaves like a symmetric diblock. The domain spacing first increases obeying the limiting scaling relation of a diblock, i.e., $D \sim \chi^{\delta}N^{\delta+1/2}$ with $\delta \simeq 0.48$.[39,40]

As in a simple AB diblock copolymer melt, the A- and B-monomers in a linear−alternating block copolymer melt try to avoid each other. However, because there are many more A-monomers in a linear A_{20}-block than in *one* A-block of the alternating block (20:1), the

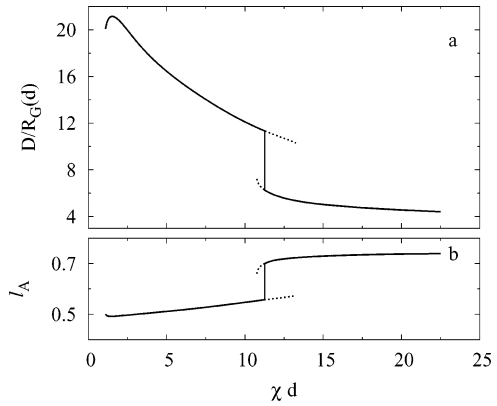

Figure 5. (a) Period D as a function of χd of the lamellar structure of the symmetric linear−alternating block copolymer A_{20}-*b*-(B-*b*-A)$_{10}$. D is expressed in units of the radius of gyration $R_G = R_G(d)$. The solid lines correspond to the stable lamellar morphology. The dotted lines correspond to the *unstable* lamellar morphology. At $\chi d = 11.27$ a phase transition occurs as the period of the lamellar structure changes discontinuously from a large to a small value. (b) Relative thickness of the lamellar A-domain l_A as a function of χd of the linear−alternating block copolymer A_{20}-*b*-(B-*b*-A)$_{10}$.

A-monomers of the linear A-block can more easily cluster together than the A-monomers of the alternating block. Hence, the A-monomers of the linear A_{20}-blocks segregate from the B- and A-monomers contained in the alternating blocks. Thus, the linear A_{20}-blocks segregate spatially from the (A-*b*-B)$_{10}$ alternating blocks. The A-rich domains are enriched with the A_{20}-blocks, whereas the B-rich domains contain relatively more of the (A-*b*-B)$_{10}$-blocks (Figure 4a). Of course, at this stage the melt is only weakly segregated.

On decreasing the temperature, the behavior quickly deviates from its initial diblock-like behavior. Instead of the A- and B-rich domains becoming purer and interfaces becoming sharper, augmented with an increase of the periodicity, the domains (especially the A-rich domains) do not become pure at all, as can be seen from the density profiles in Figure 4b,c. Moreover, the domain spacing, after an initial increase, dramatically decreases, as shown in Figure 5a presenting domain spacing vs χ parameter value. For the level of segregation shown in Figure 4b,c the phase separation is still diblock-like. However, on further cooling the A-monomers are more and more expelled from the B-rich domains, and vice versa. At very high χ values, a thin asymmetric lamellar structure is formed. Now the A-rich domains contain both the A-monomers of the alternating blocks plus the A-monomers belonging to the linear A-blocks. Such lamellae are asymmetric and have a periodicity comparable to that of a pure alternating block copolymer melt. The melt tries to adopt this morphology because it enables a maximal reduction in the number of unfavorable AB contacts; the domains become pure in this arrangement. Thus, the melt evolves from a thick lamellar to a thin asymmetric lamellar morphology. Figure 4e,f shows the intermediate segregated states of these thin asymmetric lamellae. Note that even at a comparably high χ value of $\chi d = 22.5$, the lamellae are only intermediately segregated. However, the domains have become substantially purer, and the shrinkage of the periodicity is even more pronounced.

The composition profiles demonstrate that the rearrangement of material upon cooling proceeds via a "second microphase separation" involving the segregation of the A- and B-monomers within the B-rich domain. The density profile of Figure 4c shows the development of a secondary structure, which originates from the microphase separation of the A- and B-monomers of the alternating blocks. Next, the segregation of the A- and B-monomers within B-rich domains is followed by a rearrangement of all A- and B-monomer material, leading to a significant reduction of the domain spacing. The shrinking already sets in at temperatures prior to the spinodal temperature of the pure (A-*b*-B)$_{10}$ alternating block copolymer melt, which occurs at $(\chi d)_s = 7.31194$ and a periodicity of $D^* = 5.4613 R_G(d)$. Apparently both intrinsic length scales influence the phase behavior of the linear−alternating copolymer melt, and the interplay between them results in a strong temperature dependence of the domain spacing.

When signs of a second domain structure just appear, which can be viewed as a kind of lamellar-*within*-lamellar structure, an alternative lamellar structure becomes feasible. This structure corresponds to the thin asymmetric lamellar morphology and will be denoted with L_s because its period is short in comparison to the period of the original lamellar structure, denoted as L_l. First, this lamellar structure L_s is metastable (Figure 4d), and the lamellar structure with the long periodicity (L_l) is still stable. However, on further cooling the lamellar-*within*-lamellar structure (L_l) quickly loses stability because the second domain structure introduces additional energetically unfavorable interfaces. Hence, on lowering the temperature further (Figure 4e), the thin lamellar structure L_s becomes preferable to the thick lamellar structure L_l. The actual first-order phase transition occurs at $\chi d = 11.27$. At the phase transition, the periodicity of the long lamellar structure (L_l) equals $D_l = 11.327 R_G(d)$, whereas the periodicity of the short lamellar structure (L_s) is $D_s = 6.265 R_G(d)$. Hence, the domain spacing changes by a factor of 1.81. Consequently, this phase transition can potentially form the basis for responsive materials, e.g., switching of the reflectivity as suggested in the Introduction.

The thin lamellar structure L_s remains only stable in a narrow interval of χ parameter values given by $\chi d \in [11.27, 11.80]$. At $\chi d = 11.80$ a second phase transition to hexagonally ordered cylinders occurs. Because this hexagonal structure has also a short period, we denote it with H_s. This transition from the asymmetric lamellar structure to the hexagonal structure can be easily understood on the basis of the volume fraction of the A- and B-monomers involved, which for A_{20}-*b*-(B-*b*-A)$_{10}$ corresponds to $f_A = {}^3/_4$. (Asymmetric diblock copolymer melts with $f_A \gtrsim 0.63$ adopt a hexagonal structure as their equilibrium morphology.)

To illustrate the development of the asymmetry of the lamellar structure, Figure 5b shows the relative thickness of the lamellar A-domain l_A as a function of χd. This thickness l_A is defined as the distance between two consecutive inflection points of the lamellar density profile divided by the domain spacing. Mathematically, the relative thickness of the A-domain is given by

$$l_A = \begin{cases} \dfrac{D + w_0 - v_0}{D} & v_0 > w_0 \\ \dfrac{w_0 - v_0}{D} & v_0 < w_0 \end{cases} \tag{19}$$

with $\phi_A''(z)|_{z=v,w} = 0 \wedge \phi_A'(z = v) > 0 \wedge \phi_A'(z = w) < 0 \wedge$

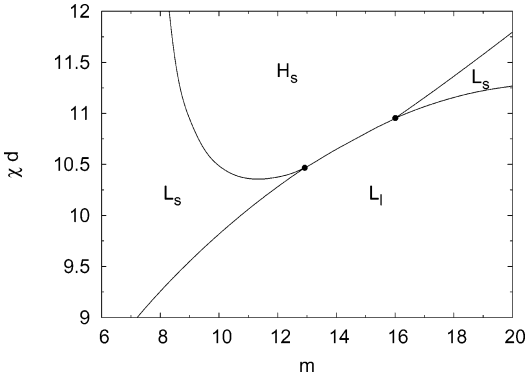

Figure 6. Phase diagram of A_m-*b*-(B-*b*-A)$_{10}$ around the long−short length scale transition. The phases are labeled L_l (lamellar with a large period), L_s (lamellar with a short period), and H_s (hexagonal ordered cylinders with a short period).

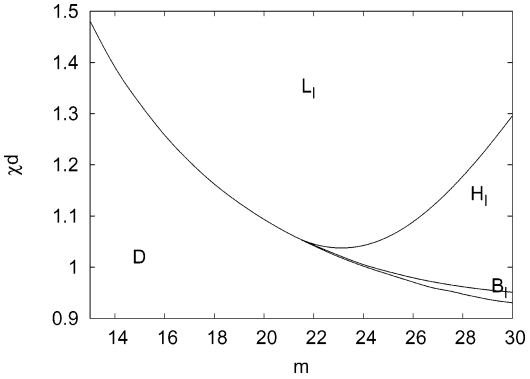

Figure 7. Phase diagram of A_m-*b*-(B-*b*-A)$_{10}$ around the ODT temperature. L_l, H_l, and B_l denote respectively lamellar, hexagonal, and spherical morphology having all a large period. D is disordered.

$v_0 = |v| \bmod D \wedge w_0 = |w| \bmod D$. Figure 5b demonstrates that before the phase transition from L_l to L_s occurs, i.e., $\chi d \lesssim 11.27$, the A- and B-rich layers have approximately the same size. Hence, the lamellar morphology is favored compared to other structures like e.g. the hexagonally ordered cylinders. At the phase transition l_A jumps discontinuously to a larger value and for increasing χd values approaches the value of $l_A = 0.75$. This is to be expected because for larger segregations the relative thickness of the lamellar A-domain must approach the A-monomer volume fraction $f_A = {}^3/_4$. At $\chi d = 11.80$ a phase transition from thin lamellae to hexagonally ordered cylinders occurs because the asymmetric lamellae become unstable compared to the hexagonally ordered cylinders.

3.3. Phase Diagrams for $n = 10$. So far, only results for the case $m = 20$ and $n = 10$, i.e., A_{10}-*b*-(B-*b*-A)$_{20}$, are presented. Next, the analysis is extended by examining the phase behavior for a wider range of A-block lengths (m) and temperatures (χd). The number of repeat units of the alternating block will still be fixed at $n = 10$. The results are presented in the phase diagrams of Figures 6 and 7. The first one is most interesting as it presents the phase behavior in the temperature range where the transition from the long to the short domain spacing occurs. As shown, this transition is from thick lamellae either to thin lamellae, followed by a second transition to hexagonally ordered cylinders with a short periodicity, or directly to hexagonally ordered cylinders.

The phase transition from thick lamellae directly to hexagonally ordered cylinders ($L_l \rightarrow H_s$) occurs in a window of m values ending in two triple points. At the triple points, given by (m, χd) = (12.92, 8.61) and (m, χd) = (16.01, 9.86), the L_l, L_s, and H_s phases all have the same free energy. The second phase diagram shows the behavior of these linear−alternating block copolymer melts around the ODT temperature. For values of $m \gtrsim 21.5$ the melt behaves similar to that of a diblock melt. The following sequence of phase transitions occurs

$$D \rightarrow B_l \rightarrow H_l \rightarrow L_l \rightarrow L_s \rightarrow H_s \qquad (20)$$

where D, B_l, H_l, and L_l refer to the disordered, the spherical, the hexagonal, and the lamellar structures, respectively. They all have periodicities comparable to those of a diblock melt with a degree of polymerization of $N = (2n + m)d$. Eventually on cooling further also the phase transitions $L_l \rightarrow L_s \rightarrow H_s$ (for $m \simeq 22$) occur. Because we have not analyzed the low-temperature behavior systematically for $m > 20$, these systems are not included in the first phase diagram (Figure 6).

For values of $m \lesssim 21.5$, i.e., for lengths of the linear A-block comparable to or smaller than the length of the alternating (A- *b*-B)$_{10}$-block, the behavior of the melt is different from that of a diblock melt: no cubic or hexagonal morphologies appear. Instead, a direct transition from the disordered to the lamellar structure occurs. For linear A-blocks smaller than $m \lesssim 21.5$ we find the following sequence of transitions

$$D \rightarrow L_l(\rightarrow L_s) \rightarrow H_s \qquad (21)$$

It depends on the value of m whether the L_s phase appears in "between" the L_l and H_s phase, as discussed above.

The ODT and the spinodal temperatures, previously calculated using RPA in ref 17, are virtually identical; within the accuracy of the graph the ODT and the spinodal-curve fall on top of each other. For $m \gtrsim 21.5$ they are distinguishable. Accurately establishing the ODT temperature for $m \lesssim 21.5$ proved to be somewhat problematic as convergence problems arose. On approaching the ODT temperature, i.e., reducing χd in small steps, the amplitudes of the density functions become small, and as a consequence the convergence rates drop. Hence, the establishment of the ODT temperatures is difficult. However, for values down to $m = 13$ the calculations are still sufficiently accurate. For smaller values of m the calculation around the ODT was insufficiently accurate.

At $m \simeq 21.5$ the phase boundaries between lamellar and hexagonal, hexagonal and spherical, and the ODT converge. Moreover, the amplitudes of the density functions become very small. This is an indication for a second-order transition; thus, a critical point should be located at $m \simeq 21.5$.

For values smaller than $m \lesssim 10$ complex structures like bi- or tricontinuous gyroid ($Ia\bar{3}d$ and $I4_132$) or rectangular structures like $p4mm$, $p2mm$, and $c2mm$ might become feasible around the ODT. For such values of m one enters the range of volume fractions where the complex $Ia\bar{3}d$ structure is anticipated to be stable (see e.g. refs 44−46). So far, we have only considered "effective" volume fractions for which the classical morphologies occur, i.e., the lamellar, hexagonal, or spherical structures.

Finally, we show in Figure 8 the density profile corresponding to a hexagonal cylindrical structure of a A_{12}-*b*-(B-*b*-A)$_{10}$ at $\chi d = 12.8125$. It clearly shows that the "structure-*within*-structure", already discussed in

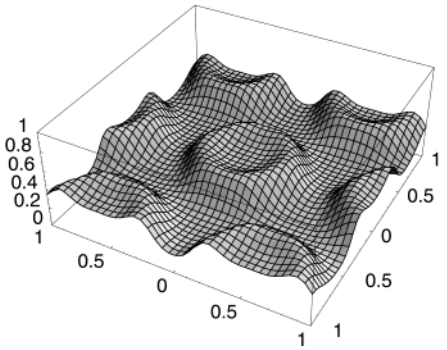

Figure 8. B-density surface of hexagonally ordered cylinders for the linear−alternating block copolymer A_{12}-*b*-(B-*b*-$A)_{10}$ and $\chi d = 12.8125$.

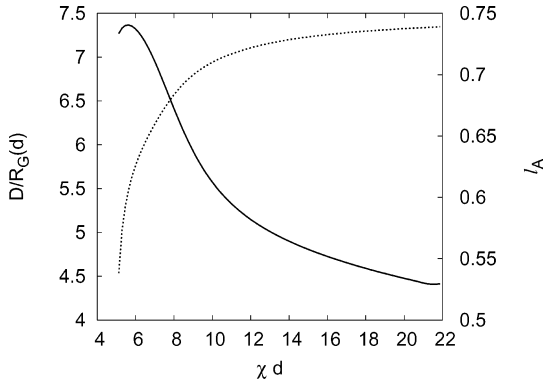

Figure 9. Period D and relative thickness l_A of the A-domain as a function of χd of the lamellar structure of the symmetric linear−alternating block copolymer A_4-*b*-(B-*b*-$A)_2$. D is expressed in units of the radius of gyration $R_G = R_G(d)$. The solid line corresponds to the periodicity of the lamellar structure, and the dotted line corresponds to the relative thickness of the A-domain.

the case of the lamellar morphology, also occurs for the hexagonal cylindrical structure. At this value of the χd the structure is already metastable against the thin hexagonal cylindrical structure as can be seen in the phase diagram (Figure 6). It is expected to be stable if the linear block is chemically different from the alternating block, i.e., C_m-*b*-(B-*b*-$A)_n$, instead of A_m-*b*-(B-*b*-$A)_n$.

3.4. Phase Diagrams for $n = 2$. Finally, we consider the A_m-*b*-(B-*b*-$A)_2$ block copolymers as the first nontrivial linear−alternating block copolymers having two intrinsic length scales. The case $n = 1$ corresponds to asymmetric triblock copolymers $A_mB_1A_1$ having one length scale only. The phase behavior of a triblock copolymer melt is similar to that of a diblock copolymer melt, and its phase diagram is topologically equivalent to that of a diblock.[32,47,48]

For the case A_m-*b*-(B-*b*-$A)_{10}$ ($n = 10$), discussed before, there is a substantial difference between the two intrinsic lengths leading to a strong temperature dependence of the domain spacing and even to phase transitions characterized by a jump in the domain spacing. For the case $n = 2$, the difference between the two intrinsic lengths is less pronounced, i.e., $q_S/q_L \sim \sqrt{2n+m} = 2\sqrt{1+m/4}$. Hence, we anticipate a much weaker temperature dependence of the periodicity. As in the case of $n = 10$, we start our analysis by considering the symmetric linear−alternating block copolymer A_4-*b*-(B-*b*-$A)_2$. Figure 9 presents the domain spacing as well as the relative thickness of the A-domains for the lamellar structure. Around the ODT the phase behavior resembles that of a diblock as phase separation occurs with a domain spacing comparable to the size of the molecule. Note that the domain spacing is already considerably smaller than that of a diblock having equal length: $D \sim 7.5R_G(d)$ against $D_{diblock} \sim 3.2R_G(N) \approx 9.1R_G(d)$. However, it is still considerably larger than the domain spacing of an alternating tetrablock copolymer given by $D_{tetra} \sim 2.8R_G(2d) \approx 4.0R_G(d)$. Hence, the periodicity is intermediate between that of a diblock and an alternating block copolymer. At the ODT the spherical structure (B_l) occurs first, which on cooling readily transforms into hexagonally ordered cylinders followed quickly by a transition to the lamellar structures. All structures have a large domain spacing. On further cooling the domain spacing of the lamellar structure starts to decrease, resembling the behavior of the linear alternating block copolymer melt A_{20}-*b*-(B-*b*-$A)_{10}$. However, the decrease is less spectacular. Moreover, no lamellar-*within*-lamellar structure evolves, and no discontinuity in the periodicity occurs. Instead, the domain spacing gradually shrinks augmented by an increase in the relative thickness of the A-domain. Thus, on cooling the lamellae become thinner and asymmetric. As the asymmetry of the lamellar domains increases, the hexagonal cylindrical structure becomes more likely, and at $\chi d = 8.09$ indeed a phase transition from the lamellae to the hexagonally ordered cylinders occurs. Hence, the melt of linear−alternating block copolymers A_4-*b*-(B-*b*-$A)_2$ goes through the following sequence of phase transitions:

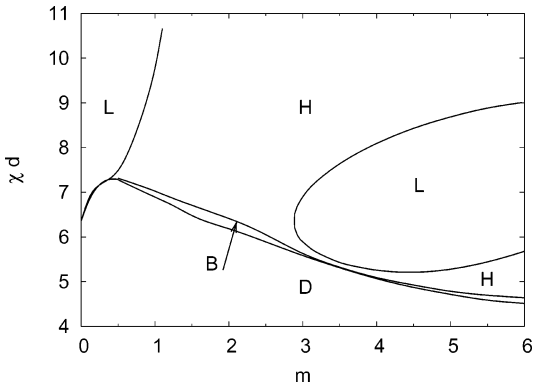

Figure 10. Phase diagram of A_m-*b*-(B-*b*-$A)_2$. The phases are labeled D (disordered), L (lamellar), H (hexagonal cylinders), and B (spherical).

$$D \rightarrow B_l \rightarrow H_l \rightarrow L \rightarrow H_s \qquad (22)$$

Here we have dropped the subscript indicating the size of the lamellar structure because its periodicity changes gradually from large to small. This is unlike the previous case (n, m) = (10, 20) where this change is abruptly, i.e., a phase transition.

Investigations into the effect of m resulted in the phase diagram shown in Figure 10. For linear−alternating block copolymers with $m > 2.89$ the melt phase behavior resembles the above-described phase behavior ($m = 4$). However, for smaller values of m no lamellar phase in between two hexagonal phases occurs. This is obviously due to the fact that on decreasing the length of the A-block (m) the difference between the two intrinsic length scales diminishes. Note that the case $m = 0$ corresponds to an alternating (tetra) block copolymer, which has only one intrinsic length scale.

Moreover for $m = 0$, due to symmetry, the ODT occurs as a critical point. Like in the case of $n = 10$, calculations around the critical point turned out to be difficult due to convergence problems, and the difference in χd between the phase lines becomes very small. This prevented us from accurately establishing the ODT, the disorder−spherical phase transition line, in the interval $m \in [0, 0.5)$. Instead for this interval the spinodal is plotted.

4. Concluding Remarks

Within the self-consistent field theory the phase behavior of a subset of linear−alternating block copolymer melts is analyzed. Because of the two intrinsic length scales, the periodicity of the self-organized structure is strongly temperature dependent. Moreover, in various cases a phase transition occurs from a lamellar morphology characterized by a large periodicity to a lamellar morphology with a small periodicity. Identifying such possibilities partially motivated the research undertaken as these kind of phase transitions could potentially form the basis for responsive materials.

One final remark concerns the subset of linear−alternating block copolymers studied. In all systems studied, the stability limit itself is governed by a single length scale; i.e., the scattering function contains a single correlation hole peak. The competition between the two intrinsic length scales only occurs in the intermediate segregation regime, in several cases leading to a first-order transition from a large length scale to a short length scale structure. Of course, for the subset of linear−alternating block copolymers systems within the bifurcation region this competition is likely to be even more pronounced as the scattering function has *two* correlation hole peaks. Consequently, the limit of stability of the disordered phase is controlled already by two length scales. Soon we hope to extend our analysis to such systems.

Acknowledgment. The authors gratefully acknowledge Profs. M. W. Matsen and J. J. M. Slot for useful discussions. J. R. de Jong is acknowledged for computational support. R.N. gratefully acknowledges financial support of the Council for Chemical Sciences of the Netherlands Organization for Scientific Research (CW-NWO).

References and Notes

(1) Breiner, U.; Krappe, U.; Abetz, V.; Stadler, R. *Macromol. Chem. Phys.* **1997**, *198*, 1051.
(2) Werner, A.; Fredrickson, G. H. *J. Polym. Sci., Part B: Polym. Lett.* **1997**, *35*, 849.
(3) Breiner, U.; Krappe, U.; Thomas, E.; Stadler, R. *Macromolecules* **1998**, *31*, 135.
(4) Ruokolainen, J.; Mäkinen, R.; Torkkeli, M.; Mäkelä, T.; Serimaa, R.; ten Brinke, G.; Ikkala, O. *Science* **1998**, *280*, 557.
(5) Ruokolainen, J.; ten Brinke, G.; Ikkala, O. *Adv. Mater.* **1999**, *11*, 777.
(6) Ruokolainen, J.; Saariaho, M.; Ikkala, O.; ten Brinke, G.; Thomas, E.; Torkkeli, M.; Serimaa, R. *Macromolecules* **1999**, *32*, 1152.
(7) Ott, H.; Abetz, V.; Alstädt, V. *Macromolecules* **2001**, *34*, 2121.
(8) Kosonen, H.; Ruokolainen, J.; Knaapila, M.; Torkkeli, M.; Serimaa, R.; Bras, W.; Monkman, A.; ten Brinke, G.; Ikkala, O. *Synth. Met.* **2001**, *121*, 1277.
(9) Mäki-Ontto, R.; de Moel, K.; Polushkin, E.; van Ekenstein, G. A.; ten Brinke, G.; Ikkala, O. *Adv. Mater.* **2002**, *14*, 357.
(10) Kosonen, H.; Ruokolainen, S. V. J.; Torkkeli, M.; Serimaa, R.; ten Brinke, G.; Ikkala, O. *Eur. Phys. J. E* **2003**, *10*, 69.
(11) Osuji, C.; Chao, C.-Y.; Bita, I.; Ober, C.; Thomas, E. *Adv. Funct. Mater.* **2002**, *12*, 753.
(12) Erukhimovich, I.; Smirnova, Y.; Abetz, V. *Polym. Sci. Ser. A* **2003**, *45*, 1093.
(13) Bates, F.; Fredrickson, G. *Phys. Today* **1999**, *52*, 32.
(14) Goldacker, T.; Abetz, V.; Stadler, R.; Erukhimovich, I.; Leibler, L. *Nature (London)* **1999**, *398*, 137.
(15) Erukhimovich, I.; Abetz, V.; Stadler, R. *Macromolecules* **1997**, *30*, 7435.
(16) Cochran, E.; Morse, D.; Bates, F. *Macromolecules* **2003**, *36*, 782.
(17) Nap, R.; Kok, C.; ten Brinke, G.; Kuchanov, S. *Eur. Phys. J. E* **2001**, *4*, 515.
(18) Nap, R.; ten Brinke, G. *Macromolecules* **2002**, *35*, 952.
(19) Helfand, E.; Tagami, Y. *J. Polym. Sci., Part B: Polym. Lett.* **1971**, *9*, 741.
(20) Helfand, E.; Tagami, Y. *J. Chem. Phys.* **1972**, *56*, 3592.
(21) Helfand, E.; Sapse, A. *J. Chem. Phys.* **1975**, *62*, 1327.
(22) Matsen, M.; Schick, M. *Phys. Rev. Lett.* **1994**, *72*, 2660.
(23) Schmid, F. *J. Phys.: Condens. Matter* **1998**, *10*, 8105.
(24) Fredrickson, G.; Ganesan, V.; Drolet, F. *Macromolecules* **2002**, *35*, 16.
(25) Matsen, M.; Schick, M. *Macromolecules* **1994**, *27*, 7157.
(26) Matsen, M. *J. Chem. Phys.* **1998**, *108*, 785.
(27) Laradji, M.; Shi, A.-C.; Noolandi, J.; Desai, R. *Macromolecules* **1997**, *30*, 3242.
(28) Nap, R. Self-Assembling block copolymer systems involving competing length scales. Ph.D. Thesis, Rijksuniversiteit Groningen, 2003.
(29) Drolet, F.; Fredrickson, G. *Phys. Rev. Lett.* **1999**, *83*, 4317.
(30) Tzeremes, G.; Rasmussen, K.; Lookman, T.; Saxena, A. *Phys. Rev. E* **2002**, *65*, 41806.
(31) Press, W.; Teukolsky, S.; Vetterling, W.; Flannery, B. *Numerical Recipes in C: The Art of Scientific Computing;* Cambridge University Press: New York, 1992.
(32) Mayes, A.; de la Cruz, M. O. *J. Chem. Phys.* **1989**, *91*, 7228.
(33) Kavassalis, T.; Whitmore, M. *Macromolecules* **1991**, *24*, 5340.
(34) Matsushita, Y.; Mogi, Y.; Mukai, H.; Watanabe, J.; Noda, I. *Polymer* **1994**, *35*, 246.
(35) Rasmussen, K.; Kober, E.; Lookman, T.; Saxena, A. *J. Polym. Sci., Part B: Polym. Phys.* **2003**, *41*, 104.
(36) Smith, S.; Spontak, R.; Satkowski, M.; Ashraf, A.; Lin, J. *Phys. Rev. B* **1993**, *47*, 14555.
(37) Spontak, R.; Smith, S. *J. Polym. Sci., Part B: Polym. Phys.* **2001**, *39*, 947.
(38) Smith, S.; Spontak, R.; Satkowski, M.; Ashraf, A.; Heape, A.; Lin, J. *Polymer* **1993**, *35*, 4527.
(39) Shull, K.; Mayes, A.; Russell, T. *Macromolecules* **1993**, *26*, 3929.
(40) Matsen, M.; Bates, F. *Macromolecules* **1996**, *29*, 1091.
(41) Benoit, H.; Hadziioannou, G. *Macromolecules* **1988**, *21*, 1449.
(42) Spontak, R.; Zielinski, J.; Lipscomb, G. *Macromolecules* **1992**, *25*, 6270.
(43) Holyst, R.; Schick, M. *J. Chem. Phys.* **1992**, *96*, 7726.
(44) Lambert, C.; Radzilowski, L.; Thomas, E. *Philos. Trans. R. Soc. London A* **1996**, *354*, 2009.
(45) Gross-Brauckmann, K. *J. Colloid Interface Sci. Phys.* **1997**, *187*, 418.
(46) Schwarz, U.; Gompper, G. *Phys. Rev. E* **1999**, *59*, 5528.
(47) Matsen, M.; Thompson, R. *J. Chem. Phys.* **1999**, *111*, 7139.
(48) Matsen, M. *J. Chem. Phys.* **2000**, *113*, 5539.

MA0356663